



The performance of phosphate removal using aluminium-manganese bimetal oxide coated zeolite: batch and dynamic adsorption studies

Ting Liu^a, Bing Chang^a, Kun Wu^{b,*}

^aCollege of Resources and Environment, Northwest A&F University, Yangling, Shaanxi 712100, China, Tel. +86 029 82202757; email: liuting8206@163.com (T. Liu), Tel. +86 029 18706813624; email: changbing1990@sina.com (B. Chang)

^bSchool of Environmental and Municipal Engineering, Xi'an University of Architecture and Technology, Xi'an, Shaanxi 710055, China, Tel. +86 029 82205652; email: tomlikeit@gmail.com

Received 7 June 2014; Accepted 18 November 2014

ABSTRACT

The discharge of wastewater containing excessive concentrations of phosphate is one of the main causes of eutrophication and can lead to serious downstream environmental effects. Adsorption technology has been recognized as a promising technology for phosphate removal from water, because of its low cost and ease of operation. In this study, we prepared an aluminum–manganese (Al–Mn) bimetal oxide-coated zeolite (AMOCZ) as a high-performance adsorbent for removing phosphate from aqueous solution. SEM and Brunauer–Emmett–Teller (BET) results showed that Al–Mn bimetal oxide was successfully coated onto zeolites, thus increasing the surface area. X-ray diffraction and Fourier transform infrared spectroscopy results demonstrated that AMOCZ has an amorphous structure and numerous active sites on its surface. The adsorption kinetic data were well fitted by the pseudo-second-order model, and the adsorption rate was retarded due to a high-concentration of phosphate. Thermodynamic results illustrated that phosphate adsorption onto AMOCZ can be satisfactorily simulated by the Langmuir model. The maximum adsorption capacity was calculated to be 7.56 mg g^{-1} at 298 K, and the adsorption process was supposed to be endothermic and spontaneous. By investigating the influences of water quality factors on phosphate adsorption, we found that phosphate removal can be facilitated under acidic conditions. In addition, phosphate adsorption is inhibited by the presence of sulfate or carbonate due to competition for active sites, whereas calcium cations are beneficial to phosphate adsorption through cation-bridging interactions. In order to evaluate the reusability of this material, we carried out reuse tests where AMOCZ was successfully used in five consecutive cycles using the recoating method for regeneration. Moreover, a satisfactory performance for phosphate removal from simulated wastewater was achieved in rapid small-scale column tests, indicating that AMOCZ has a high potential for engineering applications.

Keywords: Bimetal oxide; Zeolite; Adsorption; Phosphate

*Corresponding author.

1. Introduction

Eutrophication occurs when excess nutrients, such as nitrogen (N) and phosphorus (P), are present in aquatic ecosystems. Under certain temperature conditions, affected ecosystems typically respond by producing blue-green algae [1,2]. This production of blue-green algae is especially harmful, since this species can produce toxic chemicals which pose a serious threat to both humans and animals. In aqueous environments, pentavalent phosphorus exists in various compounds, including orthophosphate, pyrophosphate, longer chain polyphosphates, organic phosphate esters, phosphodiester, and organic phosphonates. Orthophosphate can be produced from the hydrolysis of other phosphorus compounds and can be utilized by bacteria, algae, and plants [3]. Since excessive amounts of phosphate have such a negative impact on aquatic ecosystems, it is clear that the enhanced removal of phosphate from wastewater is urgently required to deter eutrophication [2].

Various techniques have been studied for the removal of phosphate from wastewater, such as chemical precipitation [4], biological processes [5], adsorption [6], ion exchange [7], electrocoagulation [8,9], and membrane technologies [10]. Among these available approaches, the applications of ion exchange and membrane technologies have been limited due to high investment and operation costs. The use of chemical precipitation is often restricted due to the high production of waste byproduct from the water treatment process. Compared with the above treatments, the use of biological processes (i.e. activated sludge or biofilm process) is considered to be a more cost-effective and eco-friendly method. For these reasons, biological processes are now widely used for the removal of phosphate in sewage plants [11]. However, despite the positive implications of this method, the effectiveness of biological processing is dependent on multiple factors and may not always meet the discharge requirements [12]. Therefore, biological processing is usually supplemented with an additional treatment to enhance the removal of phosphate.

Another technique, the adsorption process, also has many advantages. These advantages include operation simplicity, low cost, high efficiency, and the lack of harmful byproducts. Thus, adsorption is not only a promising method as a tertiary treatment for phosphate removal in wastewater plants, but also can be easily implemented for phosphate removal from reclaimed water in small-scale treatment facilities. For this purpose, various adsorbents have been studied for phosphate removal. Yoon et al. investigated the removal of phosphate by magnetic iron oxide

nanoparticles using kinetic, equilibrium, and thermodynamic experiments [13]. Xie et al. developed a novel adsorbent, dispersed magnesium (Mg) oxide nanoflake-modified diatomite, to remove excess phosphate from eutrophic lakes [14]. They found that *in situ*-formed magnesium hydroxide ($\text{Mg}(\text{OH})_2$) could adsorb phosphate anions (PO_4^{3-} and HPO_4^{2-}) to form a surface complex due to the net positively charged surface. Li et al. synthesized nanostructured Fe–Cu binary oxides through a facile coprecipitation process and systematically evaluated its performance of phosphate removal [15]. They found that the mechanisms of phosphate adsorption were mainly attributed to the formation of inner-sphere surface complexes at the water/oxide interface as well as the replacement of surface sulfates and hydroxyl groups by the phosphate species. Su et al. explored phosphate removal performance in aqueous environments under various conditions using amorphous zirconium oxide (ZrO_2) nanoparticles as adsorbents. The ZrO_2 nanoparticles were synthesized using a simple and low-cost hydrothermal process [16]. They stated that phosphate was removed by amorphous ZrO_2 nanoparticles mainly through the adsorption mechanism of the inner-sphere complexation, in which the participation of the surface hydroxyl groups was involved. These previous studies proved that metal oxides play a key role in the development of high-performance adsorbents for phosphate removal. The abundant hydroxyl groups on the surfaces of metal oxides can respond to the high adsorption capacity towards phosphate species.

Zeolites are microporous aluminosilicate minerals, which have been commonly used as commercial adsorbents. There are two main advantages for using zeolites as an adsorbent: (1) its large surface area and high cation-exchange capacity for the facilitation of contaminant removal; (2) its good hydraulic conductivities for being used as packing materials in the fixed-bed reactors. Because of their remarkable physical and chemical properties, zeolites have been examined extensively with various modification methods for the adsorption of many kinds of contaminants, including recalcitrant organic compounds (e.g. MethylTertButylEther, MTBE) [17,18], heavy metals (e.g. Ni(II) [19], Cr(VI) [20], and arsenic (As) [21]), and nutrients (e.g. NH_4^+ -N [22]). However, previous studies revealed that natural zeolites exhibited poor adsorption performance for P, since the maximum uptake of P is less than 0.5 mg g^{-1} [23,24]. Hence, in order to use zeolites for the removal of phosphates, they must be modified to increase the active sites for phosphate binding.

In our previous studies, Al–Mn bimetal oxide was synthesized for the removal of arsenite [As(III)] and

phosphate [25,26]. It has been proved that this material has a remarkable adsorption capacity for both arsenite and phosphate. However, the adsorbent used in our previous studies was in powder form, which cannot be directly used in practical engineering projects. Hence, to improve the potential application prospect of this material in engineering fields, this study described the creation of Al–Mn bimetal oxide-coated zeolite (AMOCZ) for the adsorption of phosphate. The surface characteristics of AMOCZ were investigated using several characterization methods. The adsorption capability of AMOCZ for phosphate was evaluated through kinetic and isotherm studies. Additionally, the effects of solution pH and coexisting ions were also studied through batch experiments. Moreover, we investigated the P removal performance of regenerated AMOCZ for several consecutive operational cycles. To further evaluate the feasibility of using AMOCZ in practical engineering applications, dynamic adsorption experiments were performed using a small column packed with AMOCZ.

2. Materials and methods

2.1. Materials and adsorbent preparation

All chemicals were of analytical grade and were purchased from Beijing Chemical Company. All solutions were prepared with deionized water. Aluminum chloride (AlCl_3), potassium permanganate (KMnO_4), and manganese chloride (MnCl_2) were used for zeolite modification. Phosphate stock solutions were prepared with sodium phosphate ($\text{NaH}_2\text{PO}_4 \cdot 12\text{H}_2\text{O}$). Sodium nitrate (NaNO_3) was employed to maintain a constant ionic strength (0.01 M NaNO_3) in the solutions. Sodium hydroxide (NaOH) and hydrochloric acid (HCl) solutions were used for pH adjustments. The modified zeolites were prepared by sieving industrial-grade Na-pretreated zeolites ($\text{Na}_2\text{O} \cdot \text{Al}_2\text{O}_3 \cdot x\text{SiO}_2 \cdot y\text{H}_2\text{O}$) with particle sizes from 0.3 to 0.5 mm. The sieved zeolite particles were then rinsed using deionized water and dried in an oven prior to coating. The coating process involved dipping 20.0 g of zeolite into an 80 mL solution of $1.5 \text{ mol L}^{-1} \text{ AlCl}_3$ and $0.3 \text{ mol L}^{-1} \text{ MnCl}_2$ for 6 h. Next, 160 mL of $0.1 \text{ mol L}^{-1} \text{ KMnO}_4$ solution was slowly added to the zeolite solution under rapid stirring and a constant pH of 5.5 ± 0.1 . The resulting solution was stirred for 2 h after the addition of KMnO_4 solution. The residual solution was removed and the particles were air dried for 12 h followed by oven drying (110°C) for 3 h. The modified zeolites were rinsed with deionized water until the washing water became clear and then was dried in an oven (110°C) for 3 h. Finally, the modified zeolites

were sieved to a uniform size of 0.3–0.5 mm and stored in polyethylene bottles.

2.2. Batch and column adsorption experiments

The adsorbent dosage and contact time for all batch experiments were 5 g L^{-1} and 24 h, respectively. For kinetic experiments, 8.0 g AMOCZ was added to 1,600 mL of P solution (initial P = 10 or 50 mg L^{-1}) with an ionic strength of 0.01 M NaNO_3 at pH 7.0. The suspension was mixed with a magnetic stirrer and samples were taken at different time intervals followed by filtration with a $0.45 \mu\text{m}$ polycarbonate filter membrane. Isotherm experiments were conducted at three different temperatures (298, 308, and 318 K). In each experiment, 0.5 g of AMOCZ or zeolite was added into a set of flasks containing 100 mL of P solution with initial concentrations ranging from 5 to 100 mg L^{-1} . The ionic strength of 0.01 M NaNO_3 and the pH of 7.0 were kept constant. The flasks were shaken in a thermostatic oscillator at 170 rpm and all samples were taken and filtered after 24 h of contact. To evaluate the effects of pH, 100 mL of solutions with 50 mg L^{-1} P and different pH values (from 3.0 to 10.0) were prepared in 150 mL conical flasks. Moreover, various anions (chloride, carbonate, and sulfate) and cations (calcium and magnesium) at concentrations ranging from 0.2 to 1.0 mM were employed to investigate the effects of coexisting ions on phosphate removal. To evaluate the reuse performance of AMOCZ, the P-loaded adsorbent was recoated with Al–Mn bimetal oxide and reused in five consecutive cycles.

Rapid small-scale column (RSSC) tests were utilized, where a small glass column with a 2 cm diameter was packed with 40 cm^3 of adsorbent (the mass was 25.24 g). A peristaltic pump (Lange-580, China) was used to ensure a constant flow rate of 4 mL min^{-1} , resulting in an empty bed contact time (EBCT) of 10 min. The P concentration of the influent was 10.55 mg L^{-1} .

2.3. Analytical methods and characterizations

The concentrations of total phosphorus [P(tot)] were determined using an inductively coupled plasma atomic emission spectrometer (SCIEX Perkin Elmer Elan mode 5000, USA). Prior to analysis, the samples were acidified with 1% HNO_3 in acid-washed 10 mL glassware vessels. The surface area was measured using the BET method with a Micromeritics ASAP 2000 surface area analyzer (Micromeritics Co., USA). Samples were analyzed using a scanning electron

microscope (SEM) (Hitachi S-3500 N, Japan). X-ray diffraction (XRD) analysis was carried out on a D/Max-3A diffractometer (Rigaku Co., Japan) using Ni-filtered copper K α 1 radiation. Fourier transform infrared spectroscopy (FTIR) spectra were collected on a Nicolet 5700 FTIR spectrophotometer (Nicolet Co., USA) using transmission model. The isoelectric point (pH_{IEP}) values were determined based on the method of Bouzid et al. [27].

2.4. Data analysis

In order to investigate the potential rate-controlling step of the batch adsorption process, kinetic data were fitted with three different kinetic models, which are, respectively, presented as follows in Eqs. (1)–(4) [28–31]:

$$\log(q_e - q_t) = \log q_e - k_1 t, \quad (1)$$

(pseudo-first-order model)

$$t/q_t = t/q_e + 1/k_2 q_e^2, \quad (\text{pseudo-second-order model}) \quad (2)$$

$$q_t = (1/\beta) \times \ln t + (1/\beta) \times \ln(\alpha\beta), \quad (\text{Elovich model}) \quad (3)$$

$$q_t = k_{id} t^{0.5} + C, \quad (\text{intra-particle diffusion model}) \quad (4)$$

where t is the contact time of the adsorption experiment (h), q_e (mg g⁻¹) and q_t (mg g⁻¹) are the adsorption capacity values at equilibrium and at any time t , respectively; α (mg g⁻¹ h⁻¹) is the initial sorption rate, β (g mg⁻¹) is the desorption constant, k_1 (h⁻¹), k_2 (g mg⁻¹ h⁻¹), and k_{id} (mg g⁻¹ h^{-0.5}) are the rate constants for the aforementioned models, respectively.

To provide quantitative information for adsorption isotherms, these data were fitted by the Langmuir, Freundlich, and Dubinin–Radushkevich (D–R) isotherm models, respectively, (Eqs. (5)–(8)) [32,33]:

$$q_e = \frac{q_m b C_e}{1 + b C_e}, \quad \text{Langmuir model} \quad (5)$$

$$q_e = K_F C_e^{1/n}, \quad \text{Freundlich model} \quad (6)$$

$$\ln q_e = \ln q_m - k_{ads} \varepsilon^2 \quad (7)$$

$$\varepsilon = RT \ln \left(1 + \frac{1}{C_e} \right), \quad \text{D–R model} \quad (8)$$

where C_e is the equilibrium P concentration in the solution (mg L⁻¹), q_e is the equilibrium P concentration in the solid adsorbent (mg g⁻¹), q_m is the maximum adsorption capacity (mg g⁻¹), K_F is a constant related to the adsorption capacity (mg^{1-1/n} L^{1/n} g⁻¹), b is a constant related to the adsorption energy (L g⁻¹), n is a constant related to the adsorption energy, k_{ads} is a constant related to adsorption energy, ε is the polyani potential, R is the gas constant (8.314 kJ mol⁻¹ K⁻¹), and T is the temperature (K). The mean free energy (E_{DR}) of adsorption was calculated from the k_{ads} value using the following equation:

$$E_{DR} = -(2k_{ads})^{-0.5} \quad (9)$$

To further evaluate the thermodynamic feasibility of the process and to study the nature of the adsorption process, the thermodynamic constants, standard free energy change (ΔG), enthalpy change (ΔH), and entropy change (ΔS) were calculated using Eqs. (10)–(11) [34],

$$\Delta G = \Delta H - T\Delta S \quad (10)$$

$$\ln K = -\frac{\Delta H}{RT} + \frac{\Delta S}{R} \quad (11)$$

where K is the equilibrium constant related to the Langmuir constant b , which can be determined using the following equation:

$$K = b \times 55.5 \quad (12)$$

where the value of 55.5 corresponds to the molar concentration of the solvent (water) [35].

The adsorption performance of a fixed-bed column is usually evaluated by the characteristics of breakthrough curves, which can be obtained by plotting the dimensionless value C_t/C_0 (C_t and C_0 represent the adsorbate concentrations in the effluent and the influent, respectively) vs. time or effluent volume. Total amounts of adsorbed adsorbate can be calculated with the specific flow rate and the influent concentration by the following equation:

$$q_{tot} = Q \int_0^{t_{tot}} C_{ad} dt = Q \int_0^{t_{tot}} (C_0 - C_t) dt \quad (13)$$

where q_{tot} , Q , C_{ad} , and t_{tot} are the total amounts of adsorbed P (mg L⁻¹), volumetric flow rate (L h⁻¹), adsorbed P concentration (mg L⁻¹), and total time of flow (h), respectively. The integral in Eq. (13) is equal

to the area above the breakthrough curve. q_{eq} (mg g^{-1}) refers to the total or equilibrium uptake of P per unit mass of adsorbent, which is determined according to the following equation:

$$q_{eq} = \frac{q_{tot}}{m} \quad (14)$$

where m (g) is the amount of adsorbent.

The Thomas equation is one of the most frequently used models for interpreting column data. According to this model, it is supposed that the adsorption process not only follows the Langmuir isotherm for equilibrium, but also obeys the second-order reversible reaction kinetics. This model is applicable in the absence of internal and external diffusion limitation, and its linearized form is given by Eq. (15) [36]:

$$\ln \left(\frac{C_0}{C_t} - 1 \right) = \left(\frac{k_{Th} q_0 m}{Q} - k_{Th} C_0 t \right) \quad (15)$$

where k_{Th} ($\text{L h}^{-1} \text{mg}^{-1}$) is the Thomas rate constant and q_0 is the adsorption capacity (mg g^{-1}). Hence, k_{Th} and q_0 can be obtained by the slope and intercept from a plot of $\ln(C_0/C_t - 1)$ vs. t .

3. Results and discussion

3.1. Surface characterizations

The surface morphologies of raw zeolite and AMOCZ are illustrated in Fig. 1. Fig. 1(a) depicts the surface structure of the raw zeolite, which has cracks and needle-like particles aggregated on its rough surface. Fig. 1(b) exhibits that the zeolite particle was evenly coated with Al–Mn bimetal oxides after modification. It also shows that the porous layer of Al–Mn bimetal oxides was formed by the aggregation of numerous nanosized particles, and the coating process did not block the macropores at the surface. The described surface modification increased the BET surface area of the zeolite particles from 23.47 to 47.83 $\text{m}^2 \text{g}^{-1}$. The collected data indicate that the surface modification process can enlarge the surface area of zeolite, which may benefit its adsorption performance. While the surface area of zeolite was increased upon modification, its mean pore size decreased from 73.8 to 70.7 nm. This decrease in pore size may result from the coating of Al–Mn bimetal oxide onto the inside walls of the micropores within the zeolite.

The XRD spectra of raw zeolite and AMOCZ are illustrated in Fig. 2. As shown in Fig. 2(a), the main component of raw zeolite is clinoptilolite associated

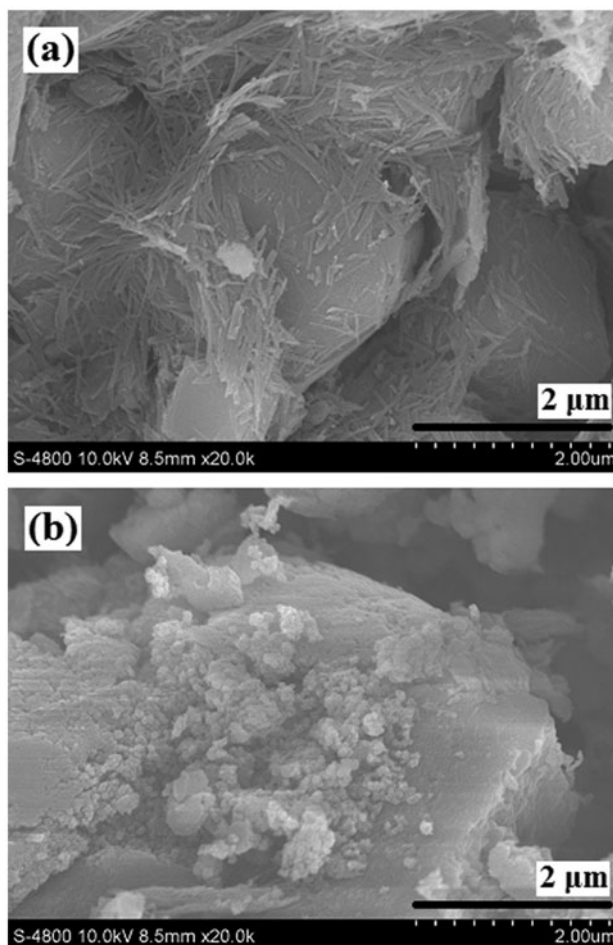


Fig. 1. SEM images of (a) raw zeolite and (b) AMOCZ.

with cristobalite, sanidine, and stilbite. Contrastively, the XRD spectrum of AMOCZ was quite different from that of raw zeolite, for which most of the peaks referring to zeolite decreased (Fig. 2(b)). In addition, a new peak appeared at 20° , indicating the existence of aluminum hydroxide (AlOOH) onto the surface. No Mn oxide was observed within the XRD spectra, which can be ascribed to the low content of Mn on the surfaces.

FTIR analysis was used to gather information regarding the active sites on zeolite surfaces. The FTIR spectra of raw zeolite and AMOCZ are shown in Fig. 3. According to previous studies [37], bands in the regions of $1,200\text{--}950 \text{ cm}^{-1}$ and $420\text{--}500 \text{ cm}^{-1}$ can be attributed to the Si–O–Si and Si–O–Al vibrations. The broad band centered at approximately $3,440 \text{ cm}^{-1}$ and the bending vibration at $1,640 \text{ cm}^{-1}$ are characteristic of hydroxyl groups (–OH) and water (H_2O), respectively. Both curves contained the four characteristic peaks mentioned above, which agreed well with the

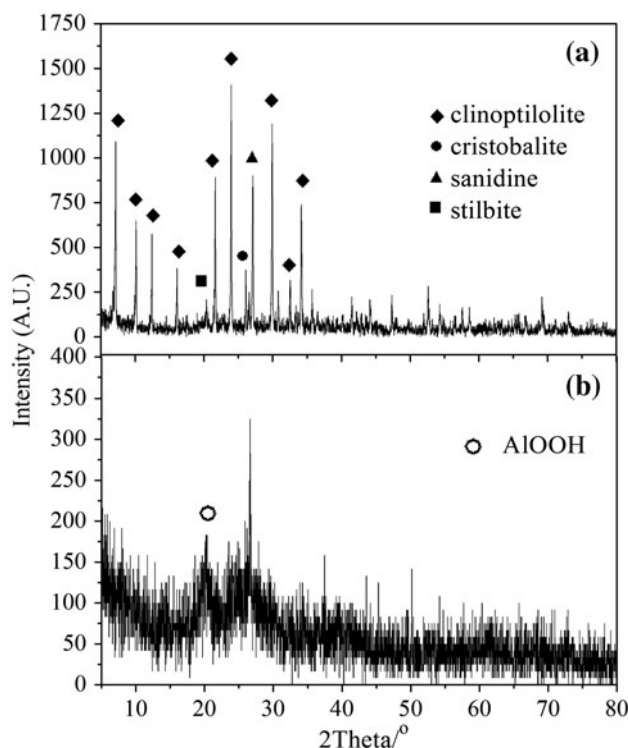


Fig. 2. XRD spectra of (a) raw zeolite and (b) AMOCZ.

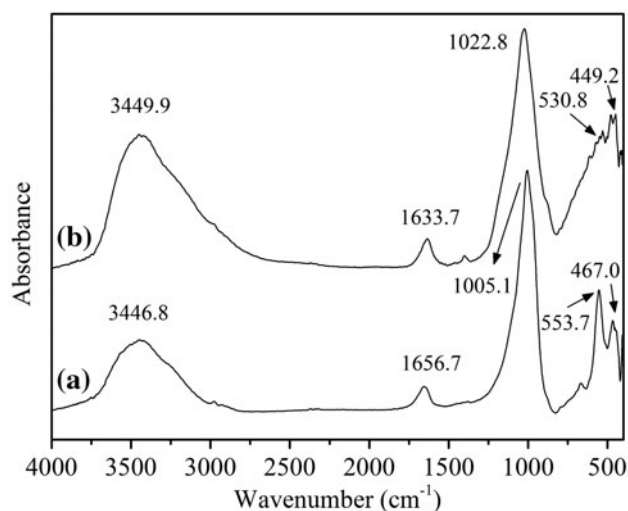


Fig. 3. FTIR spectra of raw zeolite and AMOCZ.

structural features of zeolite materials. However, it is noted that the intensity of the $-OH$ peak was increased after modification, indicating that the coating of Al-Mn bimetal oxide created more available active sites on the zeolite surface. Additionally, after modification, there was a noticeable shape change in the sharp peak at

553.7 cm^{-1} , which was shifted to 530.8 cm^{-1} . The intensity of this peak also decreased significantly. It has been reported that bands in the $500\text{--}800\text{ cm}^{-1}$ region can be assigned to pseudo-lattice vibrations, which are insensitive to the nature of zeolite, such as the channel cations and the Si/Al ratio [37]. Thus, it is suggested that the coating process can change the zeolite surface characteristics significantly. Based on the characterization results, it can be concluded that AMOCZ has an amorphous structure and numerous available hydroxyl groups on its surface [26].

3.2. Adsorption kinetics and isotherms

It is well known that a rapid adsorption rate is imperative to achieve a satisfactory adsorption performance. As shown in Fig. 4, a contact time of 1.5 h was sufficient for achieving most of (95.1%) the total P amount (1.90 mg g^{-1}) adsorbed onto AMOCZ at initial $P = 10\text{ mg L}^{-1}$. Alternatively, 85.3% of the total P uptake was reached after 14 h of contact at $P = 50\text{ mg L}^{-1}$. From these data, it can be established that the adsorption rate may be reduced by the increase in P concentration. In contrast, the equilibrium of P adsorption onto unmodified Al-Si zeolite was reached after 8 h (initial $P = 12\text{ mg L}^{-1}$) [38], suggesting that AMOCZ may possess a higher adsorption rate towards P than the artificial Al-Si zeolite. To obtain more useful information regarding the process of P adsorption onto AMOCZ, the obtained kinetic data were fitted by the pseudo-first-order, pseudo-second-order, Elovich, and intra-particle diffusion models (from Fig. 5(a)–(d)), which are, respectively, presented as Eqs. (1)–(4).

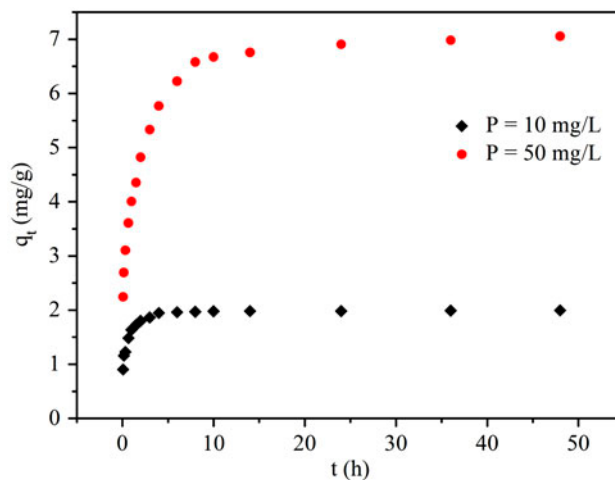


Fig. 4. The uptake of phosphate (calculated as P) onto AMOCZ at different time intervals.

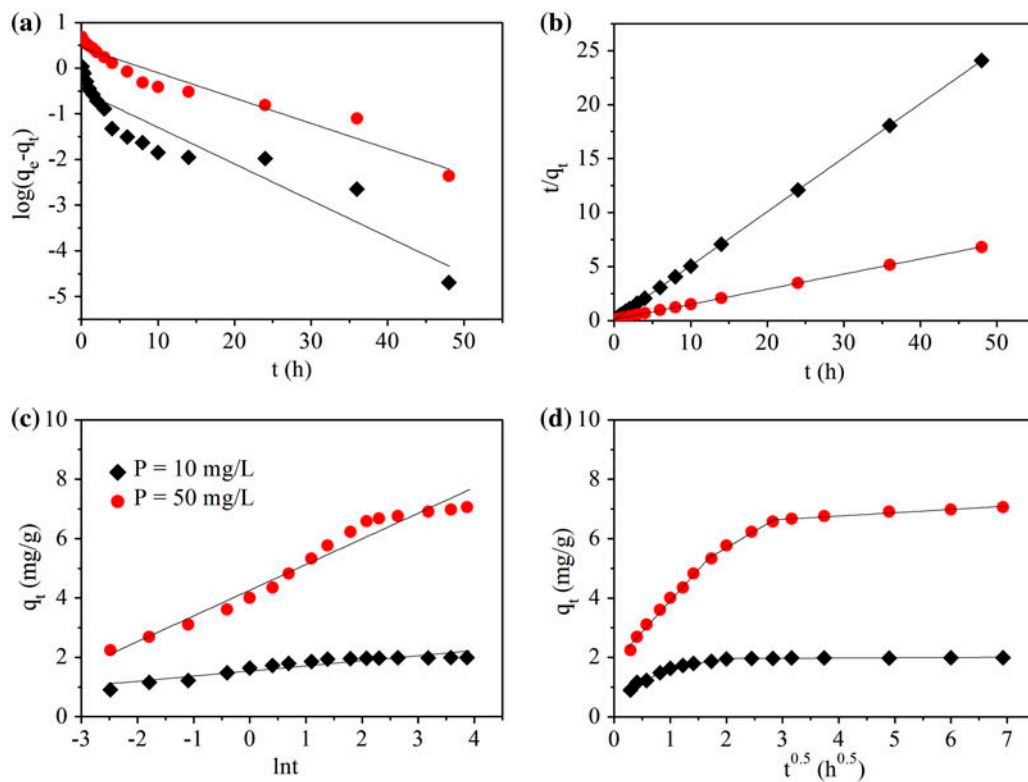


Fig. 5. The fitting of kinetic data using (a) the pseudo-first-order, (b) pseudo-second-order, (c) Elovich, and (d) intra-particle diffusion models.

Fig. 5(a) and (b) illustrate that the kinetic data were better fitted by the pseudo-second-order model ($R^2 > 0.99$) than by the pseudo-first-order model ($R^2 < 0.94$). The satisfactory application of the pseudo-second-order model suggested that a chemisorption reaction involving valence forces may limit the sharing or exchange of electrons between phosphate anions and the adsorbent [39]. Table 1 lists the parameters of the two kinetic models for phosphate adsorption onto AMOCZ. According to the pseudo-second-order model, the rate constant values (k_2) of adsorption decreased from 2.9 to 0.2 $\text{g mg}^{-1} \text{h}$ as the initial concentration of P increased from 10 to 50 mg L^{-1} .

Because the larger k_2 value means the slower adsorption rate, it is probable that a longer contact time might be required to reach the equilibrium at a higher initial P concentration [40]. The equilibrium adsorption amounts (q_e) were determined to be 2.00 and 7.13 mg g^{-1} at P concentrations of 10 and 50 mg L^{-1} , respectively. It is indicated that higher initial concentrations of P may result in greater uptake of P. Fig. 5(c) shows that the kinetic data were also fitted well by the Elovich model at P = 50 mg L^{-1} ($R^2 = 0.96$). The Elovich model has proven to be suitable for highly energetic heterogeneous systems. However, the applicability of this model declined when P

Table 1

Parameters of the pseudo-first-order, pseudo-second-order, and Elovich kinetic models for the adsorption of phosphate onto AMOCZ

Initial concentrations (mg L^{-1})	Pseudo-first-order			Pseudo-second-order			Elovich		
	k_1 (h^{-1})	q_e (mg g^{-1})	R^2	k_2 ($\text{g mg}^{-1} \text{h}^{-1}$)	q_e (mg g^{-1})	R^2	α	β	R^2
10	0.50	0.83	0.87	2.92	2.00	0.99	1,350.6	5.82	0.86
50	0.45	0.88	0.93	0.20	7.13	0.99	119.4	1.16	0.96

Note: R^2 —the square of the sample correlation coefficient.

decreased to 10 mg L^{-1} ($R^2 = 0.86$). Similar results were also obtained by Aroua et al. for the adsorption of lead(II) onto palm shell-based activated carbon [41]. The parameters of α and β for the Elovich model can be used to understand the adsorption process. It was reported by Teng and Hsieh that α is related to the chemisorption rate, while β is related to the surface coverage [42]. As the P concentration was increased from 10 to 50 mg L^{-1} , the α value decreased from 1350.6 to $119.4 \text{ mg g}^{-1} \text{ h}$. Alternatively, the β value decreased from 5.82 to 1.16 g mg^{-1} . The observed increase in α values and decrease in β values imply that the adsorption rate will decrease with the increase in initial P concentrations.

Finally, the kinetic data were fitted using the intraparticle diffusion model. As shown in Fig. 5(d), the data exhibited multilinear plots for the two curves, indicating that the sorption process was controlled by more than one step. It was observed that the fast adsorption stage ranged from 0 to 1 h at $P = 10 \text{ mg L}^{-1}$. This stage may be the key step for controlling the adsorption process. The slow and steady adsorption stages occurred in the periods of 1–4 h and 4–48 h, respectively. When the initial P was increased to 50 mg L^{-1} , the three adsorption steps were divided into

0–3 h, 3–8 h, and 8–48 h, respectively. From these observations, it can be confirmed that the adsorption process can be retarded at high initial P concentrations.

The adsorption isotherms onto the raw zeolite and AMOCZ were compared at $T = 298 \text{ K}$ (Fig. 6(a)). The results indicate that AMOCZ has a higher P adsorption capacity than that of raw zeolite, which is in accordance with the results of previous researches [23,24]. Additionally, Fig. 6(a) shows that the adsorption capacity of AMOCZ toward P increased with the rising of temperatures, thus confirming that the reaction is endothermic.

Fig. 6(b)–(d) present the linear fitting of the isotherm data with the Langmuir, Freundlich, and D–R isotherm models (Eqs. (5)–(9)), respectively. The corresponding parameters of these models were calculated accordingly and listed in Table 2. Based on the comparison of R^2 values, it is evident that the isotherm data were better fitted by the Langmuir model than by the other two models at different temperatures. Vasudevan et al. got the similar result when they investigated the adsorption of phosphate from aqueous solution onto graphene [43].

According to the Langmuir model, the maximum P uptake of AMOCZ (7.56 mg g^{-1}) was nearly twice as

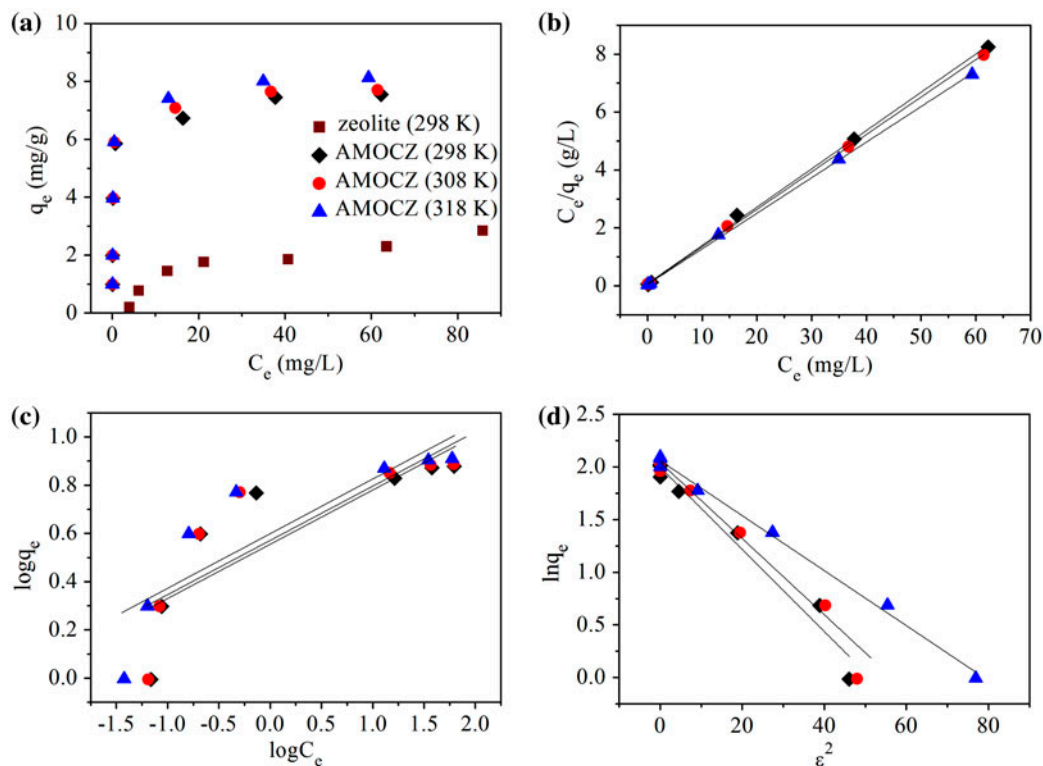


Fig. 6. (a) The adsorption amounts of P onto zeolite ($T = 298 \text{ K}$) and AMOCZ ($T = 298, 308,$ and 318 K); the fitting of isotherm data of P adsorption onto AMOCZ using the (b) Langmuir, (c) Freundlich, and (d) D–R isotherm models.

Table 2

Parameters of Langmuir, Freundlich, and D–R isotherm models for the adsorption of phosphate onto AMOCZ

Temperature (K)	Langmuir model			Freundlich model			D–R model		
	q_m (mg g ⁻¹)	b (L g ⁻¹)	R^2	K_F	n	R^2	q_m (mg g ⁻¹)	E_{dr}	R^2
298	7.56	1.80	0.99	3.59	4.45	0.72	7.36	3.58	0.97
308	7.74	2.31	0.99	3.72	4.45	0.70	7.72	3.72	0.97
318	8.14	2.50	0.99	3.97	4.42	0.75	7.84	4.38	0.99

Note: R^2 —the square of the sample correlation coefficient.

that of the raw zeolite (3.79 mg g⁻¹, fitting data not shown). The Langmuir model describes the presence of an adsorbate monolayer on a uniform surface, while the Freundlich model refers to the heterogeneity of the adsorbent surface and considers multilayer adsorption [44]. Based on the use of these two models, it can be concluded that P is adsorbed onto AMOCZ primarily via monolayer adsorption despite AMOCZ having a heterogeneous surface. In addition, the E_{DR} values for P adsorption ranged from 3.6 to 4.4 kJ mol⁻¹, where E_{DR} values below 8 kJ mol⁻¹ imply a physical adsorption. The numerical values of mean free energy were ranged between 1–8 kJ mol⁻¹ and 9–16 kJ mol⁻¹ for physical and chemical adsorptions, respectively [45].

Both ΔH and ΔS values were determined by plotting $\ln K$ vs. $1/T$ according to Eq. (11) using the Langmuir parameters at three temperatures (Fig. 7). A slope equal to $-\Delta H/R$ and an intercept equal to $\Delta S/R$ were obtained using these values. The values of ΔG were calculated using Eq. (10). It is observed that the ΔG value decreased from -11.5 to -13.1 kJ mol⁻¹ when the temperature increased from 298 to 318 K.

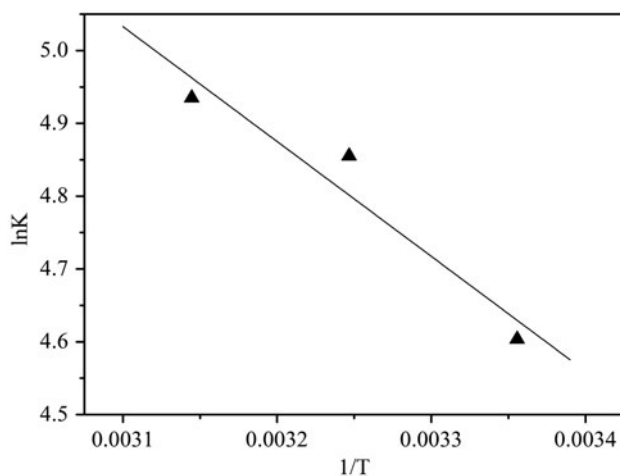


Fig. 7. Plots of $\ln K$ vs. $1/T$ (Kelvin, K) for the activation parameter.

The decrease in ΔG values resulting from elevated temperatures indicates an increase in the reaction spontaneity. The negative ΔG values and the positive ΔS value (0.08 kJ mol⁻¹ K) suggest that the adsorption process is spontaneous. Additionally, the positive ΔH value (13.1 kJ mol⁻¹) confirms that phosphate adsorption onto AMOCZ is an endothermic process. Table 3 presents a comparison of the adsorption capacities among AMOCZ and other particulate adsorbents used for removing phosphate. The comparison demonstrates that the P-adsorption capacity of AMOCZ is greater than several other mineral-based particulate adsorbents.

3.3. The effects of solution pH

Batch adsorption experiments were carried out under different pH conditions (from 3.0 to 10.0) to evaluate the effects of water quality on phosphate adsorption. Fig. 8 demonstrates that the uptake of phosphate decreased from 8.14 to 6.03 mg g⁻¹ when the initial solution pH was increased from 3.0 to 10.0. This curve suggests that alkali conditions can bring about side effects on the adsorption of phosphate. As shown in Fig. 9, the pH_{IEP} value of AMOCZ was determined to be approximately 4.2. Hence, AMOCZ surfaces are protonated at a pH < 4.2 (Eqs. (16) and (17)) and will become deprotonated at a pH > 4.2 (Eqs. (18) and (19)). The change in protonation at different pH values accounts for the variations of solution pH after adsorption. In addition, the surface of AMOCZ is positively charged at pH < 4.2 and negatively charged at pH > 4.2. Fig. 10 shows the species distributions of phosphate under different pH conditions. From these data, it is inferred that phosphate mainly exists as HPO_4^- and HPO_4^{2-} in the pH range of 3.0–10.0; and thus, the electrostatic repulsive forces between phosphate and AMOCZ may impede the adsorption in alkali conditions. However, since the uptake of phosphate decreased when the pH was increased from 3.0 to 10.0, it is supposed that electrostatic interactions may not be the dominant

Table 3
Comparison of maximum phosphate uptake between AMOCZ and other mineral-based adsorbents

Adsorbents	Particle size (μm)	P adsorption capacity (mg g^{-1})	pH	References
MCZ	300–500	7.56	7.0	This study
Calcite	N.A.	1.82	5.45	[24]
Electrochemical-modified clay tablet	<300	5.36	7.0	[46]
Fe-modified bentonite	150	3.64	7.0	[47]
Red mud granular adsorbent	150	6.64	5.0	[48]

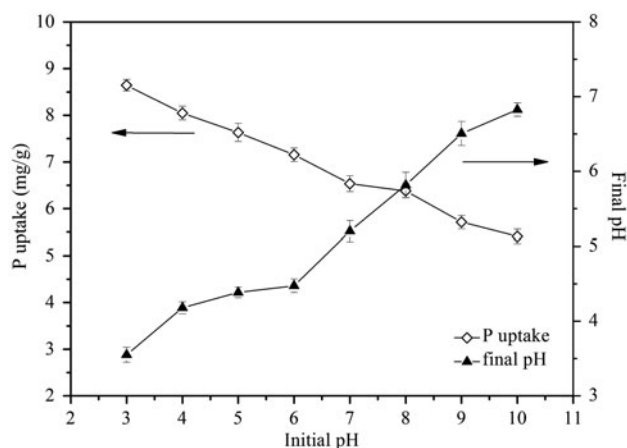


Fig. 8. Effects of solution pH on the phosphate adsorption onto AMOCZ. (Experimental conditions: ion strength = 0.01 M of NaNO_3 , adsorbent dosage = 5.0 g L^{-1} , contact time = 24 h, and rotation speed = 170 rpm.)

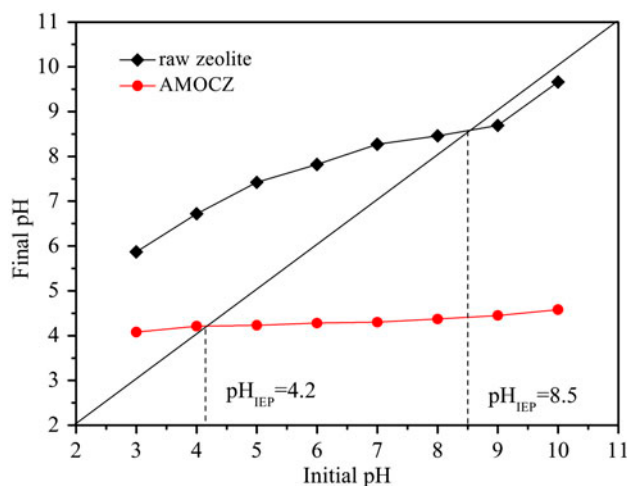


Fig. 9. Final pH variations of aqueous solution mixed with raw zeolite or AMOCZ as a function of different initial pH values. (Experimental conditions: ion strength = 0.01 M of NaNO_3 , adsorbent dosage = 5.0 g L^{-1} , contact time = 24 h, and rotation speed = 170 rpm.)

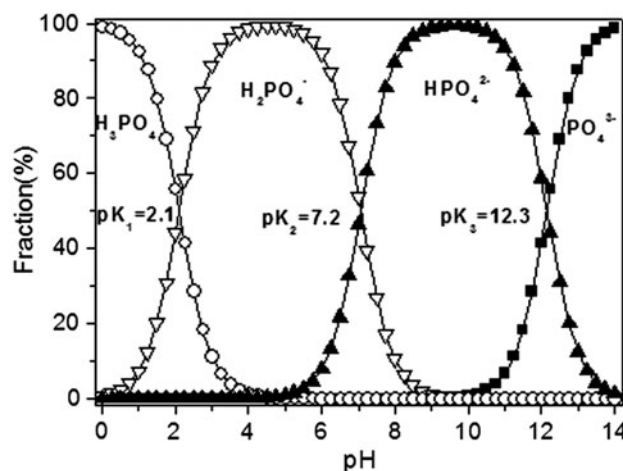
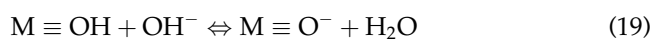
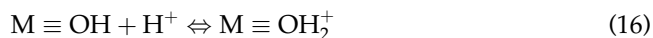


Fig. 10. Speciation distribution diagrams of phosphate with ionic strength of 0.01 M NaNO_3 .

mechanism for phosphate adsorption onto AMOCZ. Alternatively, the ion exchange between phosphate and the hydroxyl ions (OH^-) within the adsorbent surface (Eqs. (20)–(21)) can be weakened by the high concentration of OH^- in solution [49]. These reactions are in accordance with the phenomenon that the uptake of phosphate decreased with increasing pH. Therefore, the mechanism of ion exchange may play an important role in phosphate adsorption.



3.4. The effects of coexisting ions

Due to the complexity of practical wastewater, the influences of various anions and cations on phosphate adsorption were investigated accordingly. Fig. 11 illustrates that chloride ions have little influence on phosphate adsorption. However, the existence of sulfate or carbonate resulted in a drop of P uptake, especially when the carbonate concentration was greater than 4 mM or the sulfate concentration exceeded 10 mM. The inhibitory effects of the two oxyacid anions on phosphate adsorption may be ascribed to the competition for active sites [50]. Additionally, the existence of magnesium cations also posed a negative effect on phosphate adsorption. In contrast, the existence of calcium cations was beneficial to phosphate adsorption, which may be due to cation-bridging interactions [51].

3.5. Regeneration and reuse

In previous studies, NaOH solution was usually used as the eluent for the desorption of P from used adsorbents, which could then be used to adsorb P again. However, as Al oxide/hydroxide is apt to dissolve in water at both acidic and alkaline conditions, this method may not be adequate for AMOCZ. Thus, we recoated the P-loaded AMOCZ with Al–Mn bimetal oxide to restore its adsorption capacity. To verify the method used for regeneration, five cycles of consecutive regeneration and reuse were performed for P adsorption by AMOCZ (initial P of 50 mg L⁻¹, pH 7.0). As shown in Fig. 12, the P uptake increased from 6.78 to 7.13 mg g⁻¹ after the first time regeneration

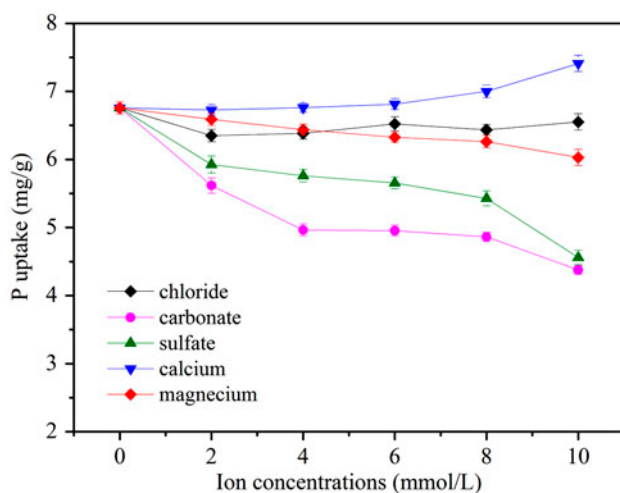


Fig. 11. Effects of coexisting ions on the phosphate adsorption onto AMOCZ. (Experimental conditions: P = 50.0 mg L⁻¹, pH 7.0, and ionic strength = 0.01 M NaNO₃.)

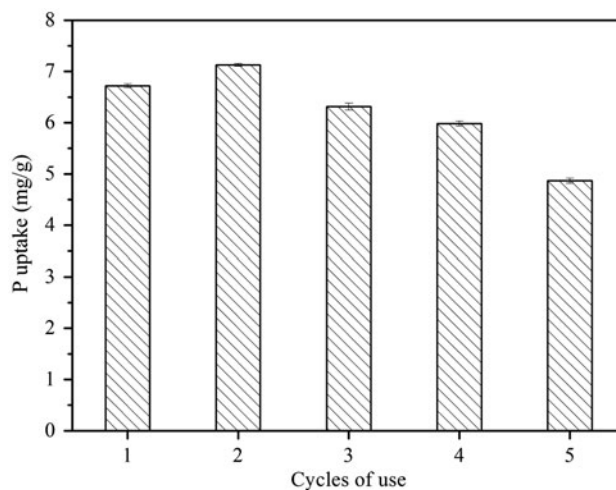


Fig. 12. P removal performance of AMOCZ (regenerated by recoating) in five consecutive cycles.

and then decreased continuously until reaching a minimum of 4.87 mg g⁻¹ in the 2nd–4th cycles. Since the activity of AMOCZ can be restored efficiently after being recoated with Al–Mn bimetal oxide without the release of phosphate, recoating may be an appropriate approach for the regeneration of AMOCZ. Furthermore, it is interesting that the adsorption amount of P was increased rather than decreased after the first regeneration cycle, which is different from the regeneration efficiency of many other adsorbents. This phenomenon is similar to the result of the previous research focused on the arsenic removal by Fe–Mn binary oxide (FMBO)-coated diatomite, which proved that the recoating process can not only compensate for the loss of active components during the adsorption process, but also enlarge the adsorption capacity toward pollutants [52].

3.6. The performance of RSSC

To further test the applicability of AMOCZ in the field, a RSSC test was performed to remove P from simulated wastewater containing phosphate. The water quality parameters were as follows: NaH₂PO₄ = 0.323 mM (P = 10.55 mg L⁻¹), NaNO₃ = 0.01 M, Na₂SO₄ = 0.1 mM, and pH 7.1–7.3. As presented in Fig. 13, the P concentration of the effluent surpassed 5% of the initial value (namely C_t/C₀ > 0.05, effluent P > 0.5 mg L⁻¹) after 10 h of operation time. According to the drainage standard of class-one A for municipal wastewater treatment plants in China (GB18918–2002), the effluent P concentration exceeded the standard prescribed at that point. Hence, the breakthrough time (t_b) was supposed to be 8.5 or 9 h, approximately. In

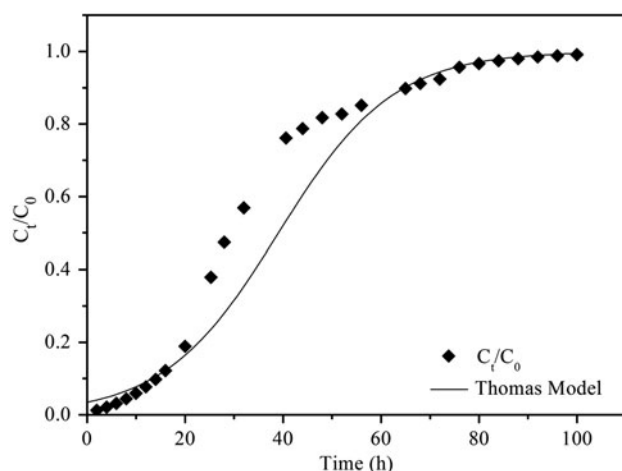


Fig. 13. Breakthrough curve of phosphate removal using a small column packed with AMOCZ. (Experimental conditions: EBCT = 10.55 min, influent P = 10.55 mg L⁻¹, pH 7.1–7.3, ionic strength = 0.01 M NaNO₃, and coexisting anion = 0.1 mM Na₂SO₄.)

addition, when the contact time reached 100 h, the effluent concentration was nearly equivalent with the influent concentration ($C_t = C_0$), indicating the exhaustion of the column. Hence, the exhaustion time (t_e) was determined as 100 h. To obtain more useful information, the dynamic experimental data were fitted by the Thomas model, which can describe the performance theory for the adsorption process in fixed-bed columns with assuming a plug flow behavior. Moreover, this model assumes Langmuir kinetics of adsorption–desorption and no axial dispersion derives with the adsorption so that the rate-driving force obeys the second-order reversible reaction kinetics [53]. According to this model, the value of k_{Th} was calculated as 0.81×10^{-2} L h⁻¹ mg, and the P uptake value at the exhaustion point ($q_{0-e} = q_{eq}$) was determined to be 3.92 mg g⁻¹ ($R^2 = 0.961$). Based on the high correlation coefficient, these experimental data were well fitted by this model, which indicated that the monolayer adsorption occurred, and hence the external and the internal diffusion are not the limiting steps during the adsorption process [54].

Considering the satisfactory performance for phosphate removal exhibited in both batch and dynamic experiments, AMOCZ has a good potential to be used as a method for removing extra P from municipal wastewater or landscape water.

4. Summary

In this study, natural zeolites were modified to enhance the removal of phosphate from aqueous solution. The results of SEM and BET showed that surface

modification could make the nanosized particles of Al–Mn bimetal oxide aggregate on the zeolite surface, and thus increase the surface area. Based on the results of XRD and FTIR, AMOCZ exhibited an amorphous structure and numerous hydroxyl groups on its surface. Through the batch and dynamic experiments, AMOCZ exhibited a satisfactory phosphate removal performance. The maximum adsorption capacity was determined to be 7.56 mg g⁻¹ at pH 7.0. Phosphate removal was favored in acidic conditions, and the P uptake could be increased to 8.64 mg g⁻¹ at pH 3.0. AMOCZ was regenerated efficiently using a recoating method without P release. The existence of calcium cations could facilitate the removal of phosphate; however, the presence of sulfate or carbonate would bring about side effects on phosphate adsorption. The results of dynamic experiment confirmed that AMOCZ can be employed for removing phosphate successfully, and the breakthrough time (eluent P > 1 mg L⁻¹) could reach 72 h with an initial P concentration of 10.55 mg L⁻¹ and EBCT of 10 min. The Thomas model was in good accordance with the dynamic experimental data, and the exhaustion capacity of the column was about 3.92 mg P per gram of AMOCZ. In the further studies, field pilot-scale dynamic experiments need to be conducted with practical wastewater, in which more operation parameters can be obtained to optimize the reactor design.

Acknowledgments

This work was supported by the Natural Science Foundation of China (Grant No. 51208415), Program for Innovative Research Team (PIRT) in Shaanxi Province (Grant No. 2013KCT-13), Key Laboratory Project of Education Department of Shaanxi Province (Grant No. 14JS042), and Major Science and Technology Program for Water Pollution Control and Treatment (Grant No. 2013ZX07310-001).

References

- [1] W.M. Lewis Jr., W.A. Wurtsbaugh, H.W. Paerl, Rationale for control of anthropogenic nitrogen and phosphorus to reduce eutrophication of inland waters, *Environ. Sci. Technol.* 45(24) (2011) 10300–10305.
- [2] D.J. Conley, H.W. Paerl, R.W. Howarth, D.F. Boesch, S.P. Seitzinger, K.E. Havens, C. Lancelot, G.E. Likens, Ecology: Controlling eutrophication: Nitrogen and phosphorus, *Science* 323(5917) (2009) 1014–1015.
- [3] D.L. Correll, The role of phosphorus in the eutrophication of receiving waters: A review, *J. Environ. Qual.* 27 (1998) 261–266.
- [4] A.H. Caravelli, C.D. De Gregorio, N.E. Zaritzky, Effect of operating conditions on the chemical phosphorus

- removal using ferric chloride by evaluating orthophosphate precipitation and sedimentation of formed precipitates in batch and continuous systems, *Chem. Eng. J.* 209(15) (2012) 469–477.
- [5] H.L. Zhang, W. Fang, Y.P. Wang, G.P. Sheng, R.J. Zeng, W.W. Li, H.Q. Yu, Phosphorus removal in an enhanced biological phosphorus removal process: Roles of extracellular polymeric substances, *Environ. Sci. Technol.* 47(20) (2013) 11482–11489.
- [6] B. Hui, Y. Zhang, L. Ye, Preparation of PVA hydrogel beads and adsorption mechanism for advanced phosphate removal, *Chem. Eng. J.* 235(1) (2014) 207–214.
- [7] A. Drenkova-Tuhtan, K. Mandel, A. Paulus, C. Meyer, F. Hutter, C. Gellermann, G. Sextl, M. Franzreb, H. Steinmetz, Phosphate recovery from wastewater using engineered superparamagnetic particles modified with layered double hydroxide ion exchangers, *Water Res.* 47(15) (2013) 5670–5677.
- [8] S. Vasudevan, G. Sozhan, S. Ravichandran, J. Jayaraj, J. Lakshmi, S.M. Sheela, Studies on the removal of phosphate from drinking water by electrocoagulation process, *Ind. Eng. Chem. Res.* 47(6) (2008) 2018–2023.
- [9] S. Vasudevan, J. Lakshmi, J. Jayaraj, G. Sozhan, Remediation of phosphate-contaminated water by electrocoagulation with aluminium, aluminium alloy and mild steel anodes, *J. Hazard. Mater.* 164(2–3) (2009) 1480–1486.
- [10] R. Shang, A.R.D. Verliefe, J.Y. Hu, Z.Y. Zeng, J. Lu, A.J.B. Kemperman, H.P. Deng, K. Nijmeijer, S.G.J. Heijman, L.C. Rietveld, Tight ceramic UF membrane as RO pre-treatment: The role of electrostatic interactions on phosphate rejection, *Water Res.* 48(1) (2014) 498–507.
- [11] S.Y. Gebremariam, M.W. Beutel, D. Christian, T.F. Hess, Research advances and challenges in the microbiology of enhanced biological phosphorus removal—A critical review, *Water Environ. Res.* 83(3) (2011) 195–219.
- [12] D. Mulkerrins, A.D.W. Dobson, E. Collieran, Parameters affecting biological phosphate removal from wastewaters, *Environ. Int.* 30(2) (2004) 249–259.
- [13] S.Y. Yoon, C.G. Lee, J.A. Park, J.H. Kim, S.B. Kim, S.H. Lee, J.W. Choi, Kinetic, equilibrium and thermodynamic studies for phosphate adsorption to magnetic iron oxide nanoparticles, *Chem. Eng. J.* 236(15) (2014) 341–347.
- [14] F.Z. Xie, F.C. Wu, G.J. Liu, Y.S. Mu, C.L. Feng, H.H. Wang, J.P. Giesy, Removal of phosphate from eutrophic lakes through adsorption by *in situ* formation of magnesium hydroxide from diatomite, *Environ. Sci. Technol.* 48(1) (2014) 582–590.
- [15] G.L. Li, S. Gao, G.S. Zhang, X.W. Zhang, Enhanced adsorption of phosphate from aqueous solution by nanostructured iron(III)–copper(II) binary oxides, *Chem. Eng. J.* 235(1) (2014) 124–131.
- [16] Y. Su, H. Cui, Q. Li, S. Gao, J.K. Shang, Strong adsorption of phosphate by amorphous zirconium oxide nanoparticles, *Water Res.* 47(14) (2013) 5018–5026.
- [17] R. Vignola, R. Bagatin, A.D.F. De Folly D’Auris, C. Flego, M. Nalli, D. Ghisletti, R. Millini, R. Sisto, Zeolites in a permeable reactive barrier (PRB): One year of field experience in a refinery groundwater—Part 1: The performances, *Chem. Eng. J.* 178 (2011) 204–209.
- [18] R. Vignola, R. Bagatin, A.D.F. De Folly D’Auris, E.P. Massara, D. Ghisletti, R. Millini, R. Sisto, Zeolites in a permeable reactive barrier (PRB): One-year of field experience in a refinery groundwater. Part 2: Zeolite characterization, *Chem. Eng. J.* 178 (2011) 210–216.
- [19] A. Nezamzadeh-Ejhieh, M. Kabiri-Samani, Effective removal of Ni(II) from aqueous solutions by modification of nano particles of clinoptilolite with dimethylglyoxime, *J. Hazard. Mater.* 260 (2013) 339–349.
- [20] G. Du, Z.H. Li, L.B. Liao, R. Hanson, S. Leick, N. Hoepfner, W.T. Jiang, Cr(VI) retention and transport through Fe(III)-coated natural zeolite, *J. Hazard. Mater.* 221–222 (2012) 118–123.
- [21] M.B. Bilici Baskan, A. Pala, Removal of arsenic from drinking water using modified natural zeolite, *Desalination* 281 (2011) 396–403.
- [22] H.B. Liu, S.C. Peng, L. Shu, T.H. Chen, T. Bao, R.L. Frost, Effect of Fe₃O₄ addition on removal of ammonium by zeolite NaA, *J. Colloid Interf. Sci.* 390 (2013) 204–210.
- [23] C. Jiang, L.Y. Jia, Y.L. He, B. Zhang, G. Kirumba, J. Xie, Adsorptive removal of phosphorus from aqueous solution using sponge iron and zeolite, *J. Colloid Interf. Sci.* 402 (2013) 246–252.
- [24] S. Moharami, M. Jalali, Removal of phosphorus from aqueous solution by Iranian natural adsorbents, *Chem. Eng. J.* 223 (2013) 328–339.
- [25] K. Wu, T. Liu, W. Xue, X.C. Wang, Arsenic(III) oxidation/adsorption behaviors on a new bimetal adsorbent of Mn-oxide-doped Al oxide, *Chem. Eng. J.* 192 (2012) 343–349.
- [26] K. Wu, T. Liu, C. Ma, B. Chang, R.G. Chen, X.C. Wang, The role of Mn oxide doping in phosphate removal by Al-based bimetal oxides: Adsorption behaviors and mechanisms, *Environ. Sci. Pollut. Res.* 21 (2014) 620–630.
- [27] J. Bouzid, Z. Elouear, M. Ksibi, M. Feki, A. Montiel, A study on removal characteristics of copper from aqueous solution by sewage sludge and pomace ashes, *J. Hazard. Mater.* 152(2) (2008) 838–845.
- [28] Y.S. Ho, G. McKay, Sorption of dye from aqueous solution by peat, *Chem. Eng. J.* 70 (1998) 115–124.
- [29] Y.S. Ho, G. McKay, Kinetic models for the sorption of dye from aqueous solution by wood, *J. Environ. Sci. Health Part B: Process Saf. Environ. Prot.* 76(B) (1998) 184–185.
- [30] D.L. Sparks, *Kinetics of Soil Chemical Processes*, Academic Press, New York, NY, 1989.
- [31] W.J. Weber Jr., J.C. Morris, Kinetics of adsorption on carbon from solution, *J. Sanitary Eng. Div.* 89(2) (1963) 31–60.
- [32] I. Langmuir, The adsorption of gases on plane surfaces of glass, mica and platinum, *J. Am. Chem. Soc.* 40 (1918) 1361–1403.
- [33] H.M.F. Freundlich, Über die adsorption in lösungen (About the adsorption in solutions), *Z. Phys. Chem. (Leipzig)* 57(A) (1906) 385–470.
- [34] M. Doula, A. Ioannou, A. Dimirkou, Thermodynamics of copper adsorption-desorption by Ca-kaolinite, *Adsorption* 6(4) (2000) 325–335.
- [35] L.T. Chiem, L. Huynh, J. Ralston, D.A. Beattie, An *in situ* ATR-FTIR study of polyacrylamide adsorption at the talc surface, *J. Colloid Interface Sci.* 297(1) (2006) 54–61.
- [36] A. Ahmad, B. Hameed, Fixed-bed adsorption of reactive azo dye onto granular activated carbon prepared from waste, *J. Hazard. Mater.* 175 (2010) 298–303.

- [37] D.W. Breck, *Zeolite Molecular Sieves Structure, Chemistry and Use*, Wiley Interscience, New York, NY, 1974.
- [38] C. Jiang, L. Jia, Y. He, B. Zhang, G. Kirumba, J. Xie, Adsorptive removal of phosphorus from aqueous solution using sponge iron and zeolite, *J. Colloid Interface Sci.* 402 (2013) 246–252.
- [39] Y.S. Ho, G. McKay, Pseudo-second order model for sorption processes, *Process Biochem.* 34 (1999) 451–465.
- [40] S. Vasudevan, J. Lakshmi, G. Sozhan, Optimization of the process parameters for the removal of phosphate from drinking water by electrocoagulation, *Desalin. Water Treat.* 12 (2009) 407–414.
- [41] M.K. Aroua, S.P.P. Leong, L.Y. Teo, C.Y. Yin, W.M.A. Wan Daud, Real-time determination of kinetics of adsorption of lead(II) onto palm shell-based activated carbon using ion selective electrode, *Bioresour. Technol.* 99 (2008) 5786–5792.
- [42] H. Teng, C. Hsieh, Activation energy for oxygen chemisorption on carbon at low temperatures, *Ind. Eng. Chem. Res.* 38(1) (1999) 292–297.
- [43] S. Vasudevan, J. Lakshmi, The adsorption of phosphate by graphene from aqueous solution, *RSC Adv.* 2 (2012) 5234–5242.
- [44] W. Rudzinski, W.A. Steele, G. Zgrablich, *Equilibria and Dynamics of Gas Adsorption on Heterogeneous Solid Surfaces*, Elsevier, Amsterdam, 1996.
- [45] M.M. Saeed, Adsorption profile and thermodynamic parameters of the preconcentration of Eu(III) on 2-thienyltrifluoroacetone loaded polyurethane (PUR) foam, *J. Radioanal. Nucl. Chem.* 256 (2003) 73–80.
- [46] S.J. Yang, Y.X. Zhao, D.H. Ding, Y.N. Wang, C.P. Feng, Z.F. Lei, Y.N. Yang, Z.Y. Zhang, An electrochemically modified novel tablet porous material developed as adsorbent for phosphate removal from aqueous solution, *Chem. Eng. J.* 220 (2013) 367–374.
- [47] M. Zamparas, A. Gianni, P. Stathi, Y. Deligiannakis, I. Zacharias, Removal of phosphate from natural waters using innovative modified bentonites, *Appl. Clay Sci.* 62–63 (2012) 101–106.
- [48] Y.Q. Zhao, Q.Y. Yue, Q. Li, X. Xu, Z.L. Yang, X.J. Wang, B.Y. Gao, H. Yu, Characterization of red mud granular adsorbent (RMGA) and its performance on phosphate removal from aqueous solution, *Chem. Eng. J.* 193–194 (2012) 161–168.
- [49] H.L. Liu, X.F. Sun, C.Q. Yin, C. Hu, Removal of phosphate by mesoporous ZrO₂, *J. Hazard. Mater.* 151 (2008) 616–622.
- [50] B.J. Pan, J. Wu, B.C. Pan, L. Lv, W.M. Zhang, L.L. Xiao, X.S. Wang, X.C. Tao, S.R. Zheng, Development of polymer-based nanosized hydrated ferric oxides (HFOs) for enhanced phosphate removal from waste effluents, *Water Res.* 43 (2009) 4421–4429.
- [51] C.C. Chusuei, D.W. Goodman, M.J. Van Stipdonk, D.R. Justes, K.H. Loh, E.A. Schweikert, Solid–liquid adsorption of calcium phosphate on TiO₂, *Langmuir* 15 (1999) 7355–7360.
- [52] K. Wu, R.P. Liu, H.J. Liu, F.F. Chang, H.C. Lan, J.H. Qu, Arsenic species transformation and transportation in arsenic removal by Fe–Mn binary oxide-coated diatomite: Pilot-scale field study, *J. Environ. Eng.* 137(12) (2011) 1122–1127.
- [53] P. Suksabye, P. Thiravetyan, W. Nakbanpote, Column study of chromium(VI) adsorption from electroplating industry by coconut coir pith, *J. Hazard. Mater.* 160 (2008) 56.
- [54] S.H. Chen, Q.Y. Yue, B.Y. Gao, Q. Li, X. Xu, K.F. Fu, Adsorption of hexavalent chromium from aqueous solution by modified corn stalk: A fixed-bed column study, *Bioresour. Technol.* 113 (2012) 114–120.